Polymer Degradation and Stability xxx (xxxx) 109707

Contents lists available at ScienceDirect

Polymer Degradation and Stability

journal homepage: www.elsevier.com/locate/polydegstab

Intumescent polybutylene succinate : Ethylenediamine phosphate and synergists

Fei Xiao [a], Gaëlle Fontaine [a], Serge Bourbigot [a, b, *]

[a] Université de Lille, CNRS, INRAE, Centrale Lille, UMR 8207 - UMET - Unité Matériaux et Transformations, Lille F-59000, France
[b] Institut Universitaire de France (IUF), Paris, France

ARTICLE INFO

Article history:
Received 19 July 2021
Received in revised form 25 August 2021
Accepted 26 August 2021

Keywords:
Polybutylene succinate
Flame retardant
Ethylenediamine phosphate
Synergism

ABSTRACT

In this work, a series of intumescent flame retarded polybutylene succinate (PBS) formulations have been developed based on ethylenediamine phosphate (EDAP) and different co-additives, *i.e.*, zinc borate, melamine borate, zinc molybdate, and aminated multiwall carbon nanotubes, at relatively low loading (10 wt.%). Among them, zinc borate endows the best synergistic flame retardant effect with EDAP in PBS. Cone calorimetry shows that addition of EDAP and zinc borate with a ratio of 8:2 (*wt: wt*) dramatically reduces the peak heat release rate (pHRR) by 57% as compared to neat PBS, indicating the excellent flame retardant efficiency of this combination used at only 10wt.%. Beside, benefitting from the incorporation of zinc borate, PBS/EDAP/ZnB exhibits excellent smoke suppression and good mechanical properties. Solid state NMR (^{11}B, ^{13}C, and ^{31}P) gives information to determine the flame retardant mechanism of EDAP and ZnB in PBS. It was found that it involves the formation of a reinforced intumescent char with highly thermally stable inorganic species, which acts as a protective physical barrier increasing the char cohesion and limiting the formation of cracks.

1. Introduction

Polybutene succinate (PBS), an emerging commercially available bio-based polyester, has been widely applied due to its controlled biodegradability, high biocompatibility, and good thermal and mechanical properties [1,2]. However, just like other non-charring aliphatic polyesters, high flammability of PBS greatly restricts its potential application in many fields [3,4]. Hence, it is imperative to enhance the fire retardancy of PBS. In the last decades, intensive efforts were made to exploit intumescent flame retardant (IFR) system for polymeric materials due to its advantages of low cost, low smoke, low toxicity, and anti-dripping during combustion [5–8]. Indeed, it currently becomes the most frequent approach to provide fire retardancy to PBS [9–12]. Generally, a typical IFR system for polyesters includes acid source (e.g., ammonium polyphosphate), blowing agent (e.g., melamine), and/or charring agent [13–16]. Currently, ammonium polyphosphate and melamine phosphate are the most commonly used acid sources in intumescent PBS systems [17]. However, they have to be incorporated at relatively high loading (more than 20%) to meet the conventional fire safety standards [18–20].

In order to explore more efficient IFR system for PBS, herein, ethylenediamine phosphate (EDAP) was incorporated into PBS matrix. EDAP is a non-halogenated intumescent flame retardant synthesized by ethylenediamine and phosphoric acid [21]. It can simultaneously act as acid source and blowing agent during the combustion due to the high content of phosphorus (19.5%) and nitrogen (17.7%) [22]. As an example, Kruger and coworkers found that the incorporation of EDAP could impart the good thermal shielding performance to low-density polyethylene/expandable graphite composite [23].

There is evidence that, during intumescence, the external environment and internal pressure caused by the evolved decomposition products can lead, in some cases, to the formation and propagation of cracks in the intumescent structure, thus reducing its barrier efficiency [24]. For this reason, suitable synergists are usually introduced into polymer intumescent systems to reinforce the thermal and mechanical properties of the protective carbonaceous layer through physical interactions and/or chemical reactions [25,26]. Recently, attention has been paid to the development of synergists to be incorporated in IFR PBS systems, including fumed silica [27], kaolinite [28], montmorillonite [29], halloysite nanotube [30], and carbon nanotube [31]. It is known that there are major advantages in using zinc borate as synergist in combination with conventional flame retardants (e.g., ammonium polyphosphate [32], magnesium hydroxide [33], and aluminum hypophosphite [34]) in halogen-free polymer systems. This is due to the formation of a pro-

* Corresponding author at: Université de Lille, CNRS, INRAE, Centrale Lille, UMR 8207 - UMET - Unité Matériaux et Transformations, Lille F-59000, France.
E-mail address: serge.bourbigot@centralelille.fr (S. Bourbigot).

https://doi.org/10.1016/j.polymdegradstab.2021.109707
0141-3910/

tective vitreous layer on the surface of burning material increasing the cohesion of residues [35,36].

In this work, the fire behavior and fire retardancy of PBS composite containing EDAP and zinc borate was evaluated by mass loss cone calorimetry (MLCC). Beside, according to our pervious works, melamine borate [37], zinc molybdate [38], and multiwall carbon nanotubes [39] were also used as potential synergists to improve the fire performance of PBS. Moreover, based on the MLCC results, the best flame retardancy were obtained with zinc borate and thus we further elucidated the combined effect of EDAP and zinc borate on smoke/thermal/mechanical properties of PBS composite. Additionally, the flame retardant mechanisms of action of PBS/EDAP/ZnB in gas and condensed phases were investigated in detail using various techniques.

2. Experimental

2.1. Materials

Polybutylene succinate (Bionolle™ 1001 MD) in pellet form was provided by Showa Denko (Japan), and ethylenediamine phosphate was supplied by CHEMOS GmbH (Germany). Zinc borate (Firebrake® ZB, $2ZnO{\bullet}3B_2O_3{\bullet}3.5H_2O$) was purchased from US Borax (USA), melamine borate was supplied by Italmatch Chemicals (Italy), zinc molybdate was purchased from ABCR Gute Chemie (Germany), aminated multiwall carbon nanotubes (NH_2-CNT, NC3152) was provided by Nanocyl S.A (Belgium). All the materials were desiccated in an oven at 80 °C overnight prior to be used.

2.2. Preparation of PBS composites

PBS and its composites (see Table 1) were prepared via melt compounding using a mixer torque rheometer (HAAKE Rheomix OS, Thermo Scientific, USA) at 140 °C for 15 min with a rotating velocity of 50 rpm. In all PBS composites, the total loading of additives was kept constant at 10 wt.%. Subsequently, the mixtures were hot-pressed at 140 °C for 15 min (under a pressure of 20 kN for 2 min and then 40 kN until the test was completed) in a plate press machine (LabPro press, Fontijne Presses, Netherlands) into special specimens for fire test (100 × 100 × 3 mm^3) and mechanical test (12.7 × 1.7 × 127 mm^3).

2.3. Characterization

2.3.1. Fire, smoke, and evolved gases analyses

Combustion performance of PBS and its composites was conducted using a Fire Testing Technology (FTT, UK) Mass Loss Cone Calorimeter (MLCC). According to the procedure defined in ASTM E 906, the heat release rate (HRR) of specimens was obtained by the thermopile on top of the chimney rather than employing the oxygen consumption principle (ASTM E-1354-90). The horizontally placed specimen with a dimension of 100 × 100 × 3 mm^3 (wrapped in aluminum foil except for the upper surface) was exposed to an external radiative heat flux of 35 kW/m^2 (distance of 25 mm between the conical heater and the sample), which corresponds to a common heat flux in a developing fire scenario [40]. During the fire test, the HRR was measured as a function of time; and four main parameters were obtained after MLCC test: time to ignition (TTI), total heat release (THR), peak of HRR (pHRR), and mass loss. Beside, some important fire safety parameters are further calculated based on the above data, such as flame retardancy index (FRI, defined in Eq. (1)), fire growth rate (FIGRA, defined as the maximum value of the function of heat release rate divided by elapsed test time), maximum average rate of heat emission (MARHE, defined as maximum value of the cumulative heat emission divided by time) [41]. Three replicated experiments were performed for each formulation to ensure the repeatability.

$$FRI = \frac{\left[THR * \left(\frac{pHRR}{TTI}\right)\right]_{Neat\ Polymer}}{\left[THR * \left(\frac{pHRR}{TTI}\right)\right]_{composite}} \quad (1)$$

The smoke release behavior was evaluated by testing the smoke opacity of evolved products during the MLCC test with a mimic standard tests [42]. The smoke density of evolved smoke was measured on the top of the chimney of MLCC using a smoke density analyzer TRDA 302 with light measurement system (Taurus Instrument, Germany). Specifically, the incident light intensity (intensity I_0, emitted by a halogen point light source) and transmitted light intensity (intensity I) were measured by a light sensor (Silizium Photoempfänger). The smoke opacity was obtained by calculating $(I_0\text{-}I)/I_0$ value [42].

Fourier Transform InfraRed (FTIR) was used in conjunction with the mass loss cone calorimeter (MLCC-FTIR) to assess the real-time composition and content of evolved gases produced during combustion [43]. Evolved products were analyzed using a FTIR spectrometer (Antaris™ Industrial Gas System (IGS), Thermo Fisher, USA). The gas picking pistol and transfer line (M&C Tech Group, Germany) were put on the top of chimney. The 2 m-long heating transfer line between MLCC and FTIR was maintained at 180 °C. Before analyzing the gases by FTIR, soot particles picked up by the pistol were filtered through two filters made of glass fibers (2 um) and ceramic (0.1 um), respectively. The optical pathway was 2 m-long and the chamber of the spectrometer was filled with dry air. The FTIR gas cell was kept at 180 °C and 652 Torr. Using the MLCC-FTIR technique, the evolved gases during combustion, such as water, carbon monoxide, and carbon dioxide, are quantified via a quantification method created by TQ Analyst software [44].

2.3.2. Solid state NMR analysis

^{11}B magic angle spinning - nuclear magnetic resonance (MAS-NMR) measurements were carried out at a frequency of 256.6 MHz on a Bruker Avance III 800 spectrometer (18.8 T) with a probe head of 3.2 mm operating at a spinning frequency of 20 kHz. The spectra were obtained with a 0.5 μs pulse length and a recycle delay of 2 s. 512 scans were accumulated. ^{11}B NMR chemical shift was referred to $NaBH_4$ at -42.06 ppm.

^{13}C CP MAS NMR experiments were conducted on a 9.4 T Bruker Avance II 400 spectrometer with a probe head of 4 mm operating at 100.6 MHz at a spinning frequency of 12.5 kHz. The high-power ^1H decoupling and ^1H-^{13}C cross-polarization (CP) NMR spectra were applied with a recycle delay of 5 s. The number of scans was 1024. The ^{13}C chemical shift was referred to tetramethylsilane at 0 ppm.

^{31}P DD MAS NMR experiments were performed on the same spectrometer (9.4 T) as above operating at 162 MHz with a recycle delay of 120 s. The analysis was carried out with a 4 mm probe head with ^1H decoupling (DD). The spectrum was recorded at MAS with a spinning frequency of 12.5 kHz. All spectra were acquired as a result of 16 scans. The ^{31}P chemical shift was referred to H_3PO_4 solution (85%) at 0 ppm.

Table 1
Formulation of PBS and its composites.

Sample	Composition [wt.%]					
	PBS	EDAP	Zinc borate	Zinc molybdate	Melamine borate	NH_2-CNT
PBS	100	0	0	0	0	0
PBS/EDAP	90	10	0	0	0	0
PBS/EDAP/ZnB	90	8	2	0	0	0
PBS/EDAP/ZnMo	90	8	0	2	0	0
PBS/EDAP/MB	90	8	0	0	2	0
PBS/EDAP/ZnB/NH_2-CNT	90	8	1	0	0	1

2.3.3. TGA and TG-FTIR analyses

Thermogravimetric analysis (TGA) was performed on a TA Instrument TGA Q5000IR with alumina crucibles under nitrogen atmosphere. 8–10 mg sample underwent an isotherm at 40 °C for one hour under nitrogen atmosphere (purge flow of 50 mL/min), then was heated from 40 to 800 °C with a constant heating rate of 10 °C/min under nitrogen atmosphere. All experiments were performed at least twice to ensure the repeatability. TG-FTIR was performed on a TA Instrument TGA Q5000IR coupled with a Thermo Scientific Nicolet iS10 FTIR spectrometer. The gas cell and transfer line were heated up at 190 °C to avoid the condensation of the evolved gases during the measurements. While heating, the real-time FTIR spectra were synchronously recorded every 10 s in a range of 4000–400 cm^{-1} with a scan number of 8.

2.3.4. Mechanical property

The tensile test was conducted to evaluate the mechanical properties of PBS and its composites using an Instron 4466 compression tension tensile tester (10KN, USA) at room temperature. Sheet specimens with a cross-section of 12.7 × 1.7 mm^2, a gauge length of 80 mm, and a total length of 127 mm were measured in the tensile test with a speed of 10 mm/min until the sample breaks. As a consequence, at least quintuplet specimens for mechanical performance were performed to ensure the repeatability of the results.

3. Results and discussion

3.1. Fire behavior

The fire performance of unfilled PBS and of its composites were evaluated by mass loss cone calorimetry (MLCC) at an external heat flux of 35 kW/m^2 (Fig. 1), and relevant combustion parameters obtained from MLCC test are summarized in Table 2. When exposed to the external heat flux, PBS burns severely with a pHRR of 401 kW/m^2, and its HRR curve shows a characteristic shape of non-charring materials [45]. The incorporation of 10 wt.% of EDAP leads to a slight reduction in pHRR (-16%) as compared to unfilled PBS. Moreover, the partial substitution of 2 wt.% EDAP by zinc borate, melamine borate or zinc molybdate results in a remarkable decrease of pHRR by 57%, 33%, 38%, respectively, in comparison with neat PBS. Beside, the HRR curves of PBS/EDAP/ZnB, PBS/EDAP/ZnMo, and PBS/EDAP/MB show two peaks. The first peak is assigned to the heat released by the combustion of pyrolysis products, the HRR reduces quickly due to the formation of intumescent char layer (visual observation). Subsequently, the HRR curves gradually rise with the increase of time, appearing the second peak, which are ascribed to the formation of cracks probably due to increasing internal pressure because of the accumulation of decomposing products. PBS/EDAP/ZnB shows the lowest pHRR value compared to the other formulations, suggesting that zinc borate performs the best among the evaluated co-additives. On this basis, aminated multiwall carbon nanotube is further considered to improve the char quality of PBS/EDAP/ZnB because there is evidence that multiwall carbon nanotube can be used to improve the flame retardancy and to suppress melt-dripping of polymers through the formation of jammed network [46]. However, the cone result reveals that the partial substitution of zinc borate with 1 wt.% aminated multiwall carbon nanotube obviously deteriorates the fire protection properties of composite (39% vs. 57% in pHRR). Indeed, the appearance of a high platform in HRR curve (Fig. 1a) suggests that it fails to form a protective char during combustion.

Note that all flame retarded PBS formulations show lower THR values than that of neat PBS (83.7 MJ/m^2). However, the THR values of all PBS composites are similar due to the prolonged burning time (see Table 2, time to flameout), which can also be seen from the broad HRR curves (Fig. 1b). Analogous conclusion is obtained from mass loss result that all PBS composites show similar char yields (Table 2), which are all higher than that of neat PBS (approximately 2%).

Additionally, the time to ignition (TTI) of PBS/EDAP is longer than that of neat PBS (125 s versus 109 s), and the reason may either be due to the fact that there is a difference in the melt flow behavior of PBS/EDAP compared to neat PBS before ignition, or the release of incombustible gases (e.g., NH_3) and/or phosphorus containing species dilutes the concentration of flammable pyrolysis products [47]. Based on the TTI, pHRR, and THR values of neat PBS and PBS composites obtained from MLCC test, flame retardancy index (FRI) was introduced to assess the flame retardancy of PBS composites (Eq. (1) and Table 2). Gener-

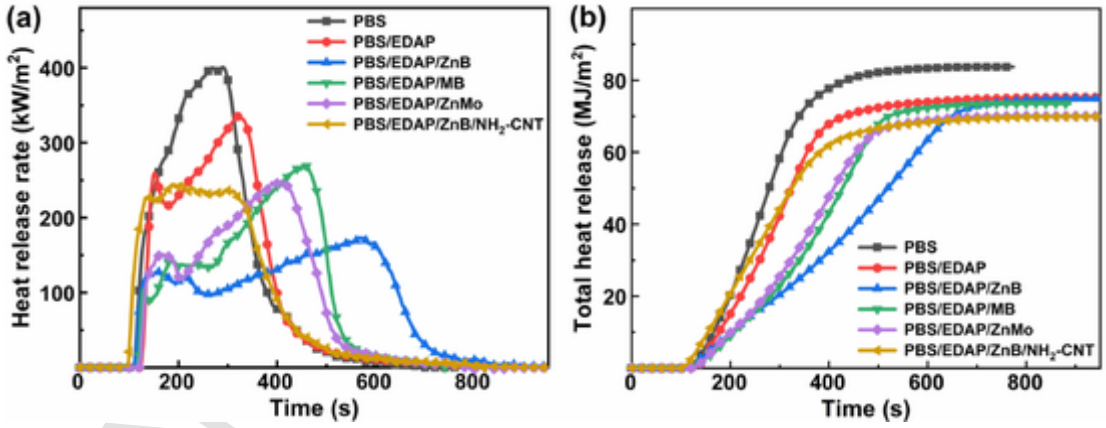

Fig. 1. (a) HRR and (b) THR curves of PBS formulations at a heat flux of 35 kW/m^2.

Table 2
MLCC results for PBS and its composites at 35 kW/m^2 heat flux.

Sample	TTI [s]	$t_{Flameout}$ [s]	pHRR[kW/m^2]	THR[MJ/m^2]	Residue[wt.%]	FIGRA[kW/(m^2s)]	FRI	MARHE[kW/m^2]
PBS	109 ± 3	493 ± 27	401 ± 8	83.7 ±1.5	2.0	1.69	/	206
PBS/EDAP	125 ± 5	476 ± 12	336 ± 3 (-16%)	74.6 ± 0.5 (-11%)	7.7	1.72 (+2%)	1.54	172 (-17%)
PBS/EDAP/ZnB	110 ± 3	737 ± 16	173 ± 22 (-57%)	74.9 ± 3.3 (-11%)	8.0	0.90 (-47%)	2.61	108 (-48%)
PBS/EDAP/MB	118 ± 7	537 ± 3	269 ± 2 (-33%)	73.4 ± 0.5 (-12%)	6.9	0.81 (-52%)	1.84	133 (-35%)
PBS/EDAP/ZnMo	122 ± 7	578 ± 21	248 ± 12(-38%)	70.1 ± 1.3 (-16%)	8.0	0.94 (-44%)	2.16	136 (-34%)
PBS/EDAP/ZnB/NH_2-CNT	100 ± 10	517 ± 5	245 ± 1 (-39%)	69.3 ± 1.0 (-17%)	8.4	1.70 (+1%)	1.81	158 (-23%)

ally, the higher the FRI value, the better the flame retardancy of PBS composite [41]. It is clear that the FRI of PBS/EDAP is only 1.54, and the introduction of co-additives can significantly improve the flame retardancy of PBS. Among them, PBS/EDAP/ZnB shows highest FRI value (2.61) than the others, indicating that zinc borate and EDAP provides the highest flame retardancy to PBS. Fire growth rate (FIGRA) was used to evaluate the fire growth and spread rates of material [48]. In opposition to FRI, a lower FIGRA value represents the slower flame spread potential and the better fire safety of material. Benefiting from the synergistic effect between EDAP and zinc borate, the FIGRA value of PBS/EDAP/ZnB is significantly reduced by 47% to 0.90 kW/(m^{2}s) compared to that of neat PBS. Beside, maximum average rate of heat emission (MARHE), another fire safety engineering parameter, was applied to assess materials by their ability to support flame spread to other objects [49]. Compared to neat PBS (206 kW/m^2), the MARHE value of PBS/EDAP/ZnB is only 108 kW/m^2, showing a 48% reduction, which is lower than that of other formulations. These results demonstrate the fact that the incorporation of zinc borate combined with EDAP obviously reduces the fire risk of PBS.

Regarding the char residues after MLCC test, neat PBS (Fig. 2a-a') burns completely and leaves no residue after the MLCC test. When EDAP is added to PBS (Fig. 2b-b'), a flat carbonaceous char with many cracks is observed, covering the surface of the sample. The poor performance (in terms of HRR) is ascribed to the low loading of EDAP (10 wt.%), which fails to develop a fully expanded char protecting the material. Interestingly, for PBS/EDAP/ZnB, a complete and smooth intumescent char layer is formed (Fig. 2c-c'), which may act as a physical barrier, inhibiting the heat and mass transfer and thereby resulting in the excellent fire retardancy. Thus, the addition of zinc borate may promotes the formation of a protective vitreous layer on the surface of burning material, which improves the cohesion of residues [35]. In the cases of PBS/EDAP/MB (Fig. 2d-d') and PBS/EDAP/ZnMo (Fig. 2e-e'), a protective carbonaceous layer is formed on the surface of the material during combustion with visible cracks and holes, leading to limited barrier effect. Beside, the combination of 1 wt.% of aminated multiwall carbon nanotubes and 1 wt.% of zinc borate to PBS/EDAP leads to the formation of a loose and discontinuous residue (Fig. 2f-f'), which is ascribed to the accumulation of multiwall carbon nanotubes on the surface of melting material restricting the formation of continuous char layer [50,51].

According to the above results, it is obvious that PBS/EDAP/ZnB shows the best flame retardant properties during combustion. Therefore, the properties and FR mechanism of this formulation is deeply investigated. Beside, the PBS/EDAP/ZnB formulation is compared to PBS/EDAP in order to evaluate the effect of ZnB, and neat PBS as a reference.

3.2. Smoke release analysis

The smoke release behavior of PBS and its composites was studied by investigating the smoke opacity of materials as a function of time during the MLCC test (Fig. 3). Generally, a low smoke opacity reflects the high visibility in a fire, which will raise the chance to escape from the fire [52]. Before the ignition, the peak values of smoke opacity of PBS/EDAP and PBS/EDAP/ZnB are 23% and 24%, respectively, which is higher than that of neat PBS (11%). This is interpreted that the addition of EDAP and zinc borate promotes the decomposition of PBS, resulting in higher smoke opacity before combustion. At ignition, the smoke opacity of PBS and PBS/EDAP as well PBS/EDAP/ZnB drops dramatically because of the burning of evolved pyrolysis products releasing mainly CO_2 and water without soot.

After ignition, the smoke opacity of neat PBS increases gradually after ignition, and reaches a peak of 21%. Beside, the smoke opacity of PBS/EDAP rises to 15% sharply and then decreases. The appearance of

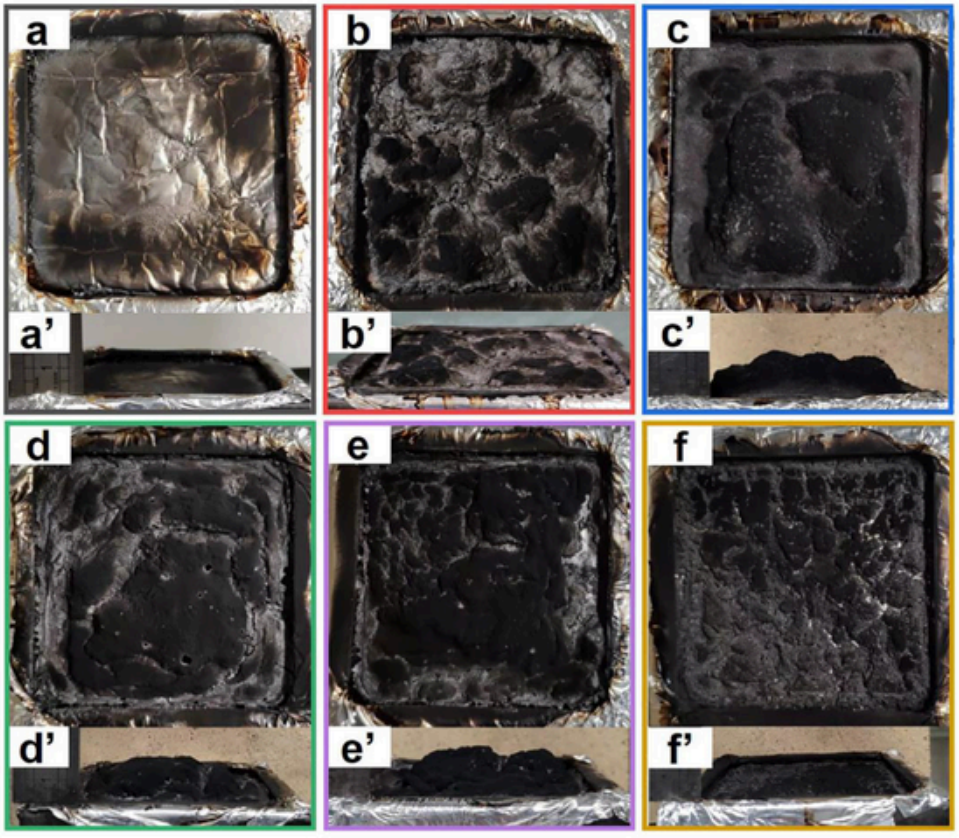

Fig. 2. Char residues of (a, a') PBS, (b, b') PBS/EDAP, (c, c') PBS/EDAP/ZnB, (d, d') PBS/EDAP/MB, (e, e') PBS/EDAP/ZnMo, (f, f') PBS/EDAP/ZnB/NH_2-CNT after MLCC test.

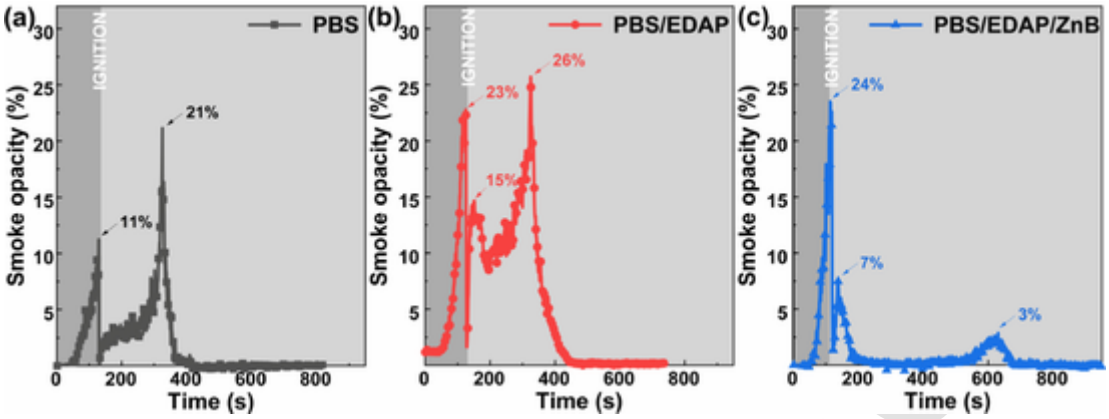

Fig. 3. Smoke opacity of (a) PBS, (b) PBS/EDAP, and (c) PBS/EDAP/ZnB during MLCC test (dark gray area: before ignition, light gray area: after ignition).

this peak is ascribed to the formation of a char. However, with the increase of testing time, the smoke opacity of PBS/EDAP climbs up to 26%, demonstrating that the formed char residue fails to retard the formation of smoke. Moreover, in the case of PBS/EDAP/ZnB, the smoke opacity reaches the peak of 7% after ignition, then quickly dropped to 0% (except for a small peak (3%) detected at around 620 s). These results indicate that the addition of zinc borate promotes the formation of protective char layer and effectively suppresses the release of smoke.

3.3. Morphology of residual char during MLCC test

The fire behaviors of neat PBS, PBS/EDAP, and PBS/EDAP/ZnB at different times during MLCC test were studied in term of char morphology (Fig. 4a-c). Neat PBS burns violently after ignition without residue. The addition of 10 wt.% EDAP leads to the formation of island-like residue on the surface of composite. However, the formed char exhibits limited flame retardancy for slowing down the combustion of underneath polymeric matrix under continuous heat flux. Partially substitut-

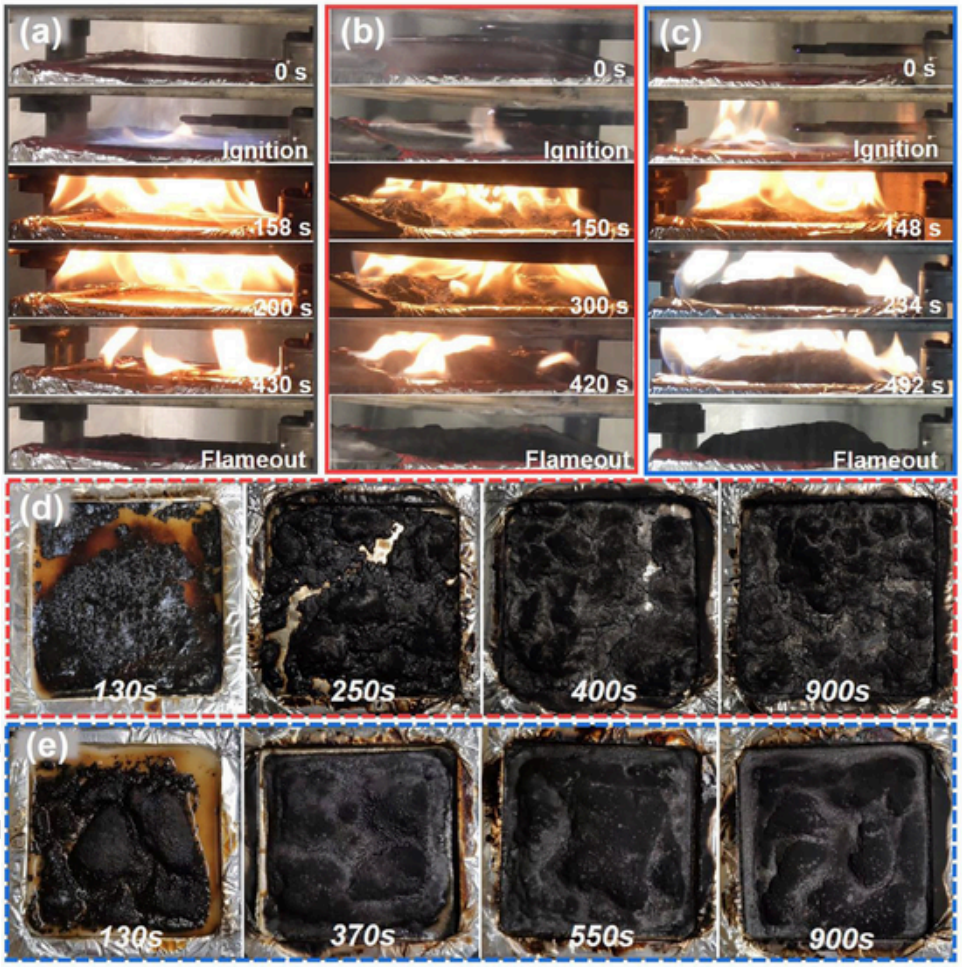

Fig. 4. Fire behavior of (a) PBS, (b) PBS/EDAP, (c) PBS/EDAP/ZnB, and top view morphological photographs of char residues of PBS/EDAP and PBS/EDAP/ZnB at different times during MLCC test.

ing EDAP with 2 wt.% zinc borate can obviously promote the formation of a protective intumescent char layer, which effectively retards the combustion of underneath matrix.

The top view morphological photographs of char residues of PBS/EDAP and PBS/EDAP/ZnB at different times (i.e., initial stage after ignition, near pHRR, HRR falling stage, and flameout stage) during MLCC test are also observed (Fig. 4d,e). It is seen that PBS/EDAP cannot form a stable and intumescent char in the early stage of decomposition and combustion. Moreover, the collapsed and discontinuous char fails to cover the surface of composite entirely during combustion (Fig. 4d), leading to the poor flame retardant efficiency of PBS/EDAP composite. On the contrary, the addition of zinc borate promotes the formation of an intumescent and compact char layer in the early stage of decomposition and combustion (Fig. 4e), and the intumescent char layer continues to expand during the combustion and completely covers the surface of the sample. As mentioned earlier, the formed intumescent char layer acts as a protective physical barrier inhibiting the transfer of heat and mass and protecting the underneath polymeric matrix.

Note that the surface char residues obtained at different times (Fig. 4d-e) were collected to characterize the chemical composition of chars and to further investigate the interactions of additives with PBS matrix in the condensed phase.

3.4. Solid state NMR analysis

To understand the reaction-to-fire of PBS/EDAP and PBS/EDAP/ZnB composites, solid state NMR test was chosen to study the chemical species of char formed at different times during the combustion process because it permits to select the observed nucleus (here, ^{11}B, ^{13}C, and ^{31}P) to get information about its surrounding [53]. Regarding the ^{13}C CP-MAS NMR spectra of EDAP, PBS/EDAP and PBS/EDAP/ZnB (Fig. 5), it is seen that EDAP shows an obvious band at 41 ppm, which is assigned to the methylene group of the ethylenediamine. Beside, ^{13}C NMR spectra of unburned PBS/EDAP and PBS/EDAP/ZnB (at 0 s) both exhibit four resonance bands located at 178, 70, 33, 30 ppm. They are contributed to the polymeric chains of PBS where the bands at 178, 70, 33, 30 ppm are assigned to the carbonyl group of succinate part (-CO-CH_2-CH_2-CO-), the methylene group of the butylene part (-O-CH_2-CH_2-CH_2-CH_2-O-), the methylene group of succinate part (-CO-CH_2-CH_2-CO-), and the methylene group of the butylene part (-O-CH_2-CH_2-CH_2-CH_2-O-), respectively [3]. For PBS/EDAP, those main characteristic bands exist during the ongoing combustion process from 0 s to 250 s. When the time reaches 400 s, the characteristic bands of PBS disappear, and a broad band centered at around 130 ppm is distinguished, corresponding to sp^2 hybridized aromatic carbon atoms, which is assigned to the carbonization of the material forming aromatic and/or polyaromatic species [54]. The formation of char is due to the dehydrogenation of aromatic species creating larger structure of polyaromatic species with low organization [40].

With respect to PBS/EDAP/ZnB, it is seen (Fig. 5b) that there is a broad band centered around 130 ppm at 370 s, indicating the formation of large aromatic/polyaromatic structure (char). At 550 s, an additional band at 178 ppm is observed, probably indicating the presence of another type of carbonyl group. Beside, the characteristic bands of aliphatic structures in PBS are continuously detected at longer time (550 s), demonstrating that the incorporation of zinc borate significantly improves the thermal-oxidative stability of PBS during combustion.

Upon heating, EDAP decomposes and releases acidic phosphates acting as char promoter, it plays an important role in the charring and formation of an intumescent char. ^{31}P NMR chemical shift was use to study the phosphorus-containing char by determining the number of bridging oxygen atoms (n) and distinguishing between phosphate units using Q^n terminology: Q^0, Q^1, Q^2, and Q^3 [55]. Before the MLCC test (0 s), the ^{31}P DD-MAS NMR spectra of EDAP, PBS/EDAP, and PBS/EDAP/ZnB (Fig. 6) shows a narrow single peak at 0 ppm, which is assigned to Q^0 site (orthophosphate type species including phosphoric acid). This band is characteristic of phosphoric acid and/or orthophosphate groups, because EDAP is an orthophosphate salt prepared by the reaction between phosphoric acid and ethylenediamine.

It is found that a twin peak at around -1 ppm is distinguished at 130s on the PBS/EDAP, corresponding to another Q^0 site probably an orthophosphate linked to aliphatic species [24]. Beside, an additional band of low intensity at around -12 ppm is detected, which is assigned to Q^1 site (orthophosphate linked to the aromatic species) and/or another Q^1 site (pyrophosphates) [40]. A broad band around -25 ~ -55 ppm is observed from 250 s, indicating the formation of amorphous phosphate-type exhibiting Q^2 and Q^3 site (probably due to the presence of metaphosphates and ultraphosphates) [56]. For PBS/EDAP/ZnB, at 130 s, the broad band between 5 and -50 ppm is characteristic of the structure found in glass or amorphous compounds, while narrow resonances are characteristic of ordered phases composed of borophosphate, zinc phosphate, phosphate glasses and so on [38,57]. Indeed, the sharp intense resonance at -30 ppm is assigned to boron phosphate as already evidenced in previous work [58]. The band at 0 ppm is attributed as above, and the band at -7.7 ppm is assigned to Q^1 site corresponding to pyrophosphate [59]. In addition, the broad band centered at -12 ppm might be assigned as above in a disordered structure and/or to zinc phosphate glass. At higher testing times for PBS/EDAP/ZnB, the intensity of band at 0 ppm decreases, and the resonances at -30 ppm increases significantly due to the formation of boron phosphate [60]. Based on the above results, it suggests that zinc borate can react with EDAP and its decomposition products during combustion. The formation of borophosphate and/or zinc phosphate glasses reinforces the

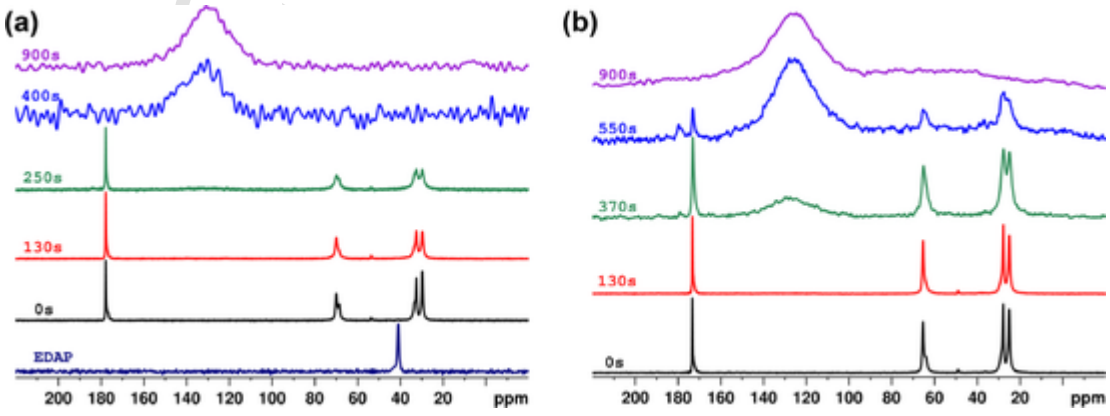

Fig. 5. ^{13}C CP-MAS ssNMR spectra of (a) PBS/EDAP and (b) PBS/EDAP/ZnB.

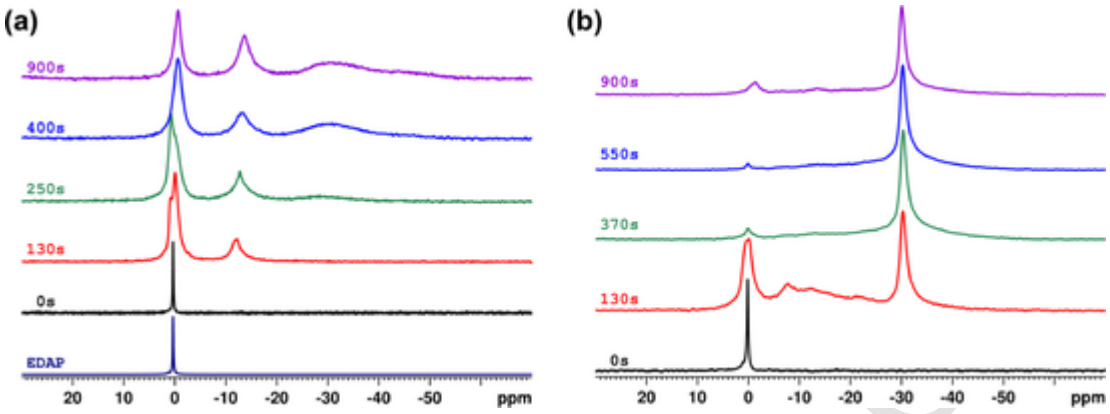

Fig. 6. ^{31}P DD-MAS ssNMR spectra of (a) PBS/EDAP and (b) PBS/EDAP/ZnB.

char structure and acts as a 'glue' providing flexibility and cohesion to the char, thereby improving the flame retardancy of the material.

^{11}B MAS NMR spectra of PBS/EDAP/ZnB are shown on Fig. 7. The spectra of unburned material (0 s) exhibit a doublet centered at 15 and 13 ppm, which is assigned to the trigonal borate (BO_3) units [38]. Beside, another band located at 1 ppm is ascribed to chemical shift of tetragonal borate (BO_4) species. With advancing burning process, the broad band assigned to BO_3 units disappears gradually, and the resonance of BO_4 units at 1 ppm is shifted to -4 ppm. This is ascribed to the formation of borophosphate (boron phosphate) [60]. Those results indicate that borates react with phosphate upon heating, leading to reinforcement in char integrity and stability [61], which is consistent with the ^{31}P DD-MAS NMR results. Further, the reaction between EDAP and zinc borate can be explained by the Lewis acid-base concept: the phosphate is the strongest or hardest Lewis base, whereas the zinc and boron are the Lewis acid [34]; accordingly, phosphate species (EDAP and its pyrolysis products) tends to react with ZnO and B_2O_3 to form zinc phosphate and borophosphate species, respectively [62].

3.5. MLCC-FTIR analysis

FTIR spectra was used to quantitatively analyze the evolved gases, such as water and carbon dioxide, in the smoke from MLCC fire test to further investigate the gas phase combustion behavior [63]. Herein, the amounts of water, carbon dioxide, and carbon monoxide evolved as a function of time during the MLCC test (Fig. 8a-c) were evaluated for PBS and its composites.

Note that the evolution curves of water and carbon dioxide show similar shapes to the HRR curve during the burning (Fig. 8a,b). For neat PBS, the evolution of water and carbon dioxide increase rapidly after ignition indicating the completed combustion. The water emission peak of PBS/EDAP is 12546 ppm, similar to that of neat PBS (12817 ppm); meanwhile the peak of water emission for PBS/EDAP/ZnB is only 7698 ppm, a 38.6% reduction compared to neat PBS. Regarding the release of carbon dioxide, neat PBS/EDAP shows an emission peak at 42428 ppm, which is lower than the release of neat PBS (47308 ppm). Moreover, the carbon dioxide emission curve of PBS/EDAP/ZnB exhibits a lower plat with a peak of 22591 ppm, which means that the formed char layer retards the combustion of material effectively.

Interestingly, the evolution of carbon monoxide is obviously different to the release of water and carbon dioxide (Fig. 8c). For neat PBS, carbon monoxide is evolved before ignition, and the corresponding maximum CO emission value is 161 ppm. Compared to neat PBS, the carbon monoxide emission of PBS/EDAP remains at a relatively high level during the combustion (peak of 250 ppm), demonstrating the incomplete combustion behavior happens during the combustion of PBS/EDAP. This phenomenon suggests a possible flame retardant mechanism occurred in the gas phase by adding EDAP in PBS [64,65]. Beside, for PBS/EDAP/ZnB, the release of carbon monoxide keeps at a low level until the flame is almost extinguished. Subsequently, a sharp evolved peak is observed at around 700 s, which is ascribed to the barrier effect of protective intumescent char layer. Those results validate the flame retardant mechanism occurred in the condensed phase.

3.6. Thermal decomposition behavior

The thermal decomposition behaviors of EDAP, zinc borate, neat PBS and its composites were analyzed by TGA under nitrogen atmosphere (Fig. 9). The related thermal parameters, including the initial degradation temperature ($T_{5\%}$, where 5 wt.% weight loss occurs), maximum degradation temperature (T_{max}), and the char yield (Y_c) at 800 °C, are listed in Table 3.

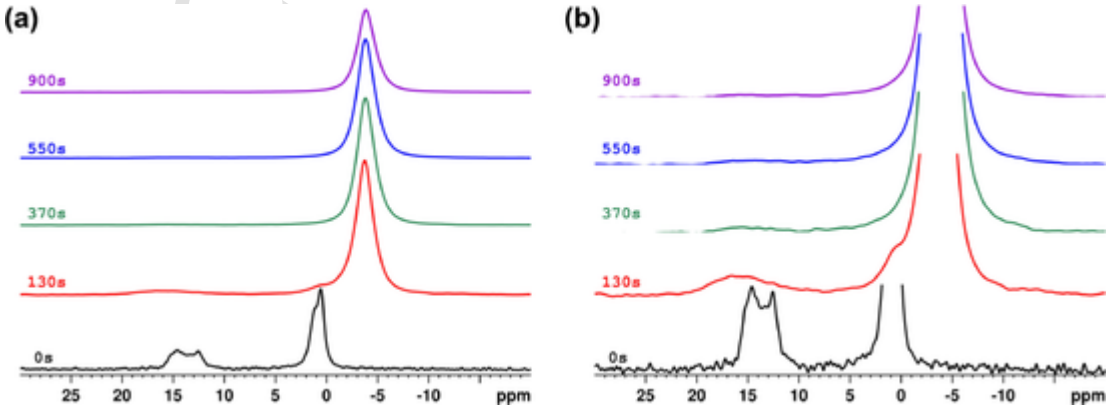

Fig. 7. ^{11}B MAS ssNMR spectra of PBS/EDAP/ZnB: (a) normal and (b) magnified.

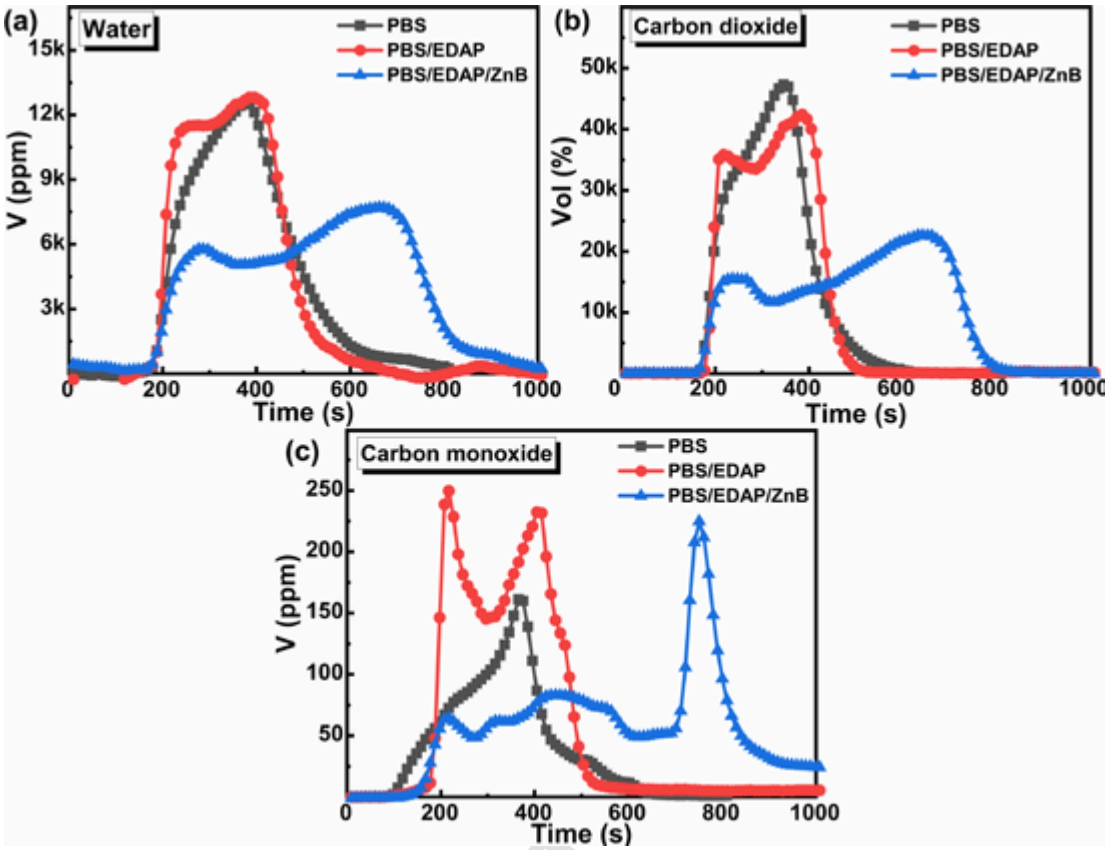

Fig. 8. Evolution of (a) water, (b) carbon dioxide, and (c) carbon monoxide for neat PBS, PBS/EDAP, and PBS/EDAP/ZnB during MLCC test.

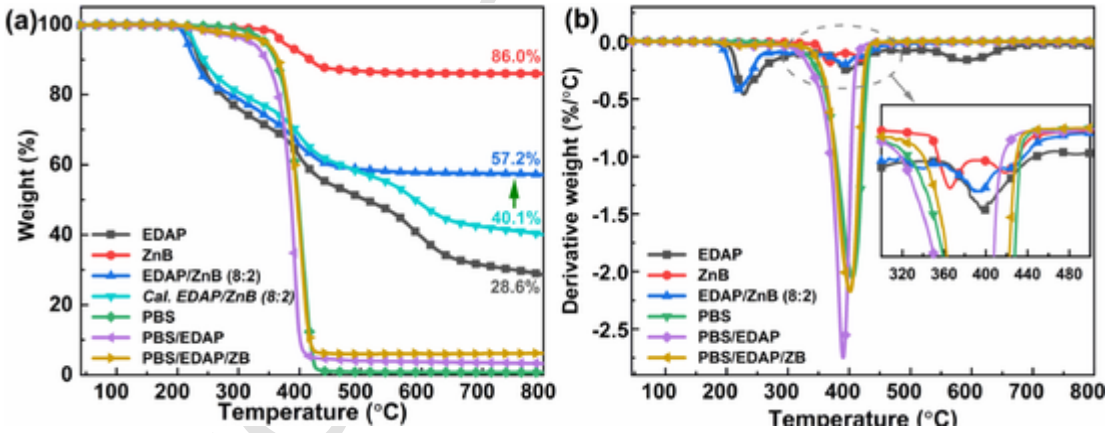

Fig. 9. (a) TGA and (b) DTG curves of EDAP, ZnB, EDAP/ZnB(8:2), calculated EDAP/ZnB(8:2), PBS and its composites under nitrogen atmosphere.

Table 3
TGA and DTG data of PBS and its composites under nitrogen atmosphere.

Sample	$T_{5\%}$ (°C)	T_{max} (°C)	*Yc* at 800°C (wt.%)
EDAP	225	238	28.6
ZB	373	377	86.0
PBS	343	401	0.8
PBS/EDAP	320	382	3.3
PBS/EDAP/ZnB	344	396	6.2

EDAP goes through a thermal decomposition in three steps, leaving 28.6 wt.% residue at 800 °C. The $T_{5\%}$ of EDAP is observed at 225 °C, implying that the decomposition of EDAP appears at a relatively low temperature [23,66]. For zinc borate, the *Yc* is as high as 86.0 wt.%, and the mainly mass loss is due to the endothermic decomposition (releasing water) of zinc borate occurred between 350 °C and 450 °C [35]. The mass loss process of zinc borate involves two overlapping dehydration reaction (Fig. 9b), including the condensation of B-OH groups and the crystallization processes [67]. The combination of EDAP and zinc borate with a mass ratio of 4:1 yields 57.2% residue (Fig. 9a), which is higher than the calculated result (40.1%, calculated from the content of additives and the experimental results of each component [24]). It means that there is an interaction between EDAP and zinc borate improving thermal stability.

It is found that neat PBS degrades from 343 °C ($T_{5\%}$), it undergoes a one-stage thermal decomposition process. Compared to neat PBS, two-stage thermal decomposition pathway exists in PBS/EDAP and PBS/EDAP/ZnB composites, occurring approximately from 225 °C to 325 °C and from 325 °C to 425 °C, respectively. The first thermal decomposition is ascribed to the earlier degradation of EDAP, which leads to ap-

proximately 4% mass loss of composites [68]. When incorporating 10 wt.% EDAP to PBS matrix, $T_{5\%}$ and T_{max} of PBS/EDAP is decreased by 23 °C and 19 °C (from 343 °C to 320 °C and from 401 °C to 382 °C, respectively), compared to that of neat PBS. Moreover, in comparison with the composite containing 10 wt.% EDAP, PBS/EDAP/ZnB exhibits the $T_{5\%}$ and T_{max} of 344 °C and 396 °C, respectively, similar to those of neat PBS, implying that the incorporation of zinc borate visibly improves the thermal stability of composite.

As far as the residue is concerned, it is clear that the addition of EDAP increases the Y_c of composite to 3.3% from 0.8% for neat PBS at 800 °C. Moreover, a higher Y_c (6.2%) is observed for PBS/EDAP/ZnB in the presence of zinc borate, indicating the better charring-forming effect. Generally, the higher residual char means positive thermal protect effect on the PBS matrix, which in turn reflects the ability to protect the PBS composites when exposed to fire.

3.7. TG-FTIR analysis

The evolved pyrolysis products of PBS and its composites were analyzed by TG-FTIR in nitrogen atmosphere to understand the decomposition behavior and possible flame-retardant mechanism of PBS composites (Fig. 10). The major evolving decomposition products of neat PBS include various ester compounds (containing monomers and hybrid dimers), tetrahydrofuran, carbon dioxide, succinic anhydride, and aliphatic ethers [69,70], which is identified by strong characteristic FTIR signals (Fig. 10a, d), such as unsaturated alkane (3000–3100 cm^{-1}), hydrocarbons (2800–3000 cm^{-1}), carbon dioxide (2300–2400 cm^{-1}), carbonyl compounds (1811–1818 cm^{-1}), aliphatic ethers (1100–1250 cm^{-1}). The FTIR spectra of evolved gas products at different times for PBS/EDAP and PBS/EDAP/ZnB are similar to those of neat PBS (Fig. 10b-d). It is speculated that some new absorption peaks, such as P = O (1250 cm^{-1}) and P-O-C (1075 cm^{-1}) may coincide with the characteristic bands of the PBS matrix [18,71]. Beside, the low loading of additives may also affect the intensity of characteristic bands.

FTIR spectra of EDAP, neat PBS, PBS/EDAP, and PBS/EDAP/ZnB at the maximum decomposition rate were also studied (Fig. 10e). For EDAP, the sharp peaks at 3330, 1626, 965, 931 cm^{-1} are ascribed to characteristic bands of ammonia (from NIST Chemistry WebBook), the broad band between 1000 and 1200 cm^{-1} is contributed to the absorbance of ammonia and phosphorus-containing species [72]. Compared to neat PBS, the peak intensity of PBS/EDAP at 909 cm^{-1} increases dramatically after the incorporation of EDAP. This phenomenon suggests that the absorption band of C-H deformation vibration of alkene is overlapped by the additional absorption of ammonia decomposed from EDAP [27]. Beside, from Fig. 10e, the maximum decomposition rate of PBS/EDAP occurs at 35.9 min (396 °C), which is earlier than that of neat PBS (37.6 min, 413 °C). This is interpreted that the addition of EDAP promotes the thermal decomposition of PBS. In contrast, the maximum decomposition rate of PBS/EDAP/ZnB occurs at 38.1 min (418 °C), indicating that the presence of zinc borate can improve the thermal stability of PBS composite. Fig. 10f-h presents the main evolved gases for PBS and its composites, such as total absorbance, carbonyl compounds (1818 cm^{-1}), and hydrocarbons (2980 cm^{-1}). It is seen that, compared to neat PBS, PBS/EDAP exhibits higher absorption intensities of the volatized products during decomposition. On the contrary, the absorption intensities of pyrolysis products significantly are reduced for PBS/EDAP/ZnB as shown in Fig. 10f-h. The reduction of pyrolysis gases verifies the thermal shielding and the smoke suppression effects of zinc borate combined with EDAP in PBS [73,74].

3.8. Flame retardant mechanisms of action

Based on above discussions, the flame retardant mechanisms of PBS/EDAP/ZnB are mainly contributed to the formation of a protective intumescent char layer (condensed phase mechanism). Specifically, EDAP mainly acts as acid source in this intumescent system and promotes the charring of PBS matrix. The decomposition of zinc borate (between 350 °C and 450 °C) produces B_2O_3, which softens at 350 °C (melting point of 450 °C) and flows above 500 °C [35,75]. It leads to the formation of a protective vitreous layer on the surface of material during combustion, thereby improving the cohesion of the residue [35]. Beside, zinc oxide, another decomposition product of zinc borate, is able to form cross-links with the flame retardant system to limit the formation of cracks and holes [76,77]. It has been proved that zinc oxide can stabilize char structure and make the char more compact [77]. Moreover, based on the solid state NMR analyses, zinc borate can react with EDAP during combustion to form thermally stable inorganic phosphate species (boronphosphate and/or zinc phosphate), which physically reinforce the char structure. The resultant intumescent char layer effectively limits the mass and heat transfer and retards the combustion of material.

3.9. Mechanical properties of PBS and its composites

The effect of EDAP and zinc borate on the mechanical properties of PBS composites was investigated using a tensile test. The stress-strain curves of PBS and its composites are showed in Fig. 11. It can be seen that the neat PBS shows the highest tensile strength than its flame retarded PBS composites. When incorporating 10 wt.% EDAP to PBS, the tensile strength of PBS/EDAP is deceased to 32.0 MPa from 39.7 MPa for neat PBS. This might be due to the poor compatibility between EDAP and PBS matrix. Analogous phenomena are widely observed in intumescent flame retardant systems that the addition of intumescent flame retardants to polymers or polymer composites with relatively high loadings often negatively affects the mechanical properties of polymer matrix [10,78]. In comparison with PBS/EDAP, the addition of zinc borate increases the tensile strength of PBS/EDAP/ZnB (33.9 MPa), thanks to the inherent rougher surface of zinc borate and the improved interfacial interaction between zinc borate and PBS matrix [79]. This result suggests that the presence of zinc borate leads to a reinforcement effect in the mechanical properties of PBS composites.

4. Conclusion

A series of halogen-free intumescent flame retardant formulations for polybutylene succinate consisting of ethylenediamine phosphate and synergists were described, and mechanism details of the mode of action for selective formulation (PBS/EDAP/ZnB) were also given in this study. Among them, zinc borate provided the best synergistic flame retardant effect with EDAP to PBS. The cone calorimeter results showed that the co-addition of EDAP and zinc borate at relatively low additive loading (10 wt.%, with a mass ratio of 8:2) permitted the reduction up to 57% of pHRR, indicating the high flame retardant efficiency. Based on the condensed phase and gas phase analyses, it can be concluded that the addition of zinc borate and EDAP promoted the formation of a reinforced intumescent char. This protective char layer effectively limited mass and heat transfer, thereby retarding the combustion. Beside, the presence of zinc borate significantly decreased the smoke release during combustion, and improved the tensile strength of composite in comparison to PBS/EDAP.

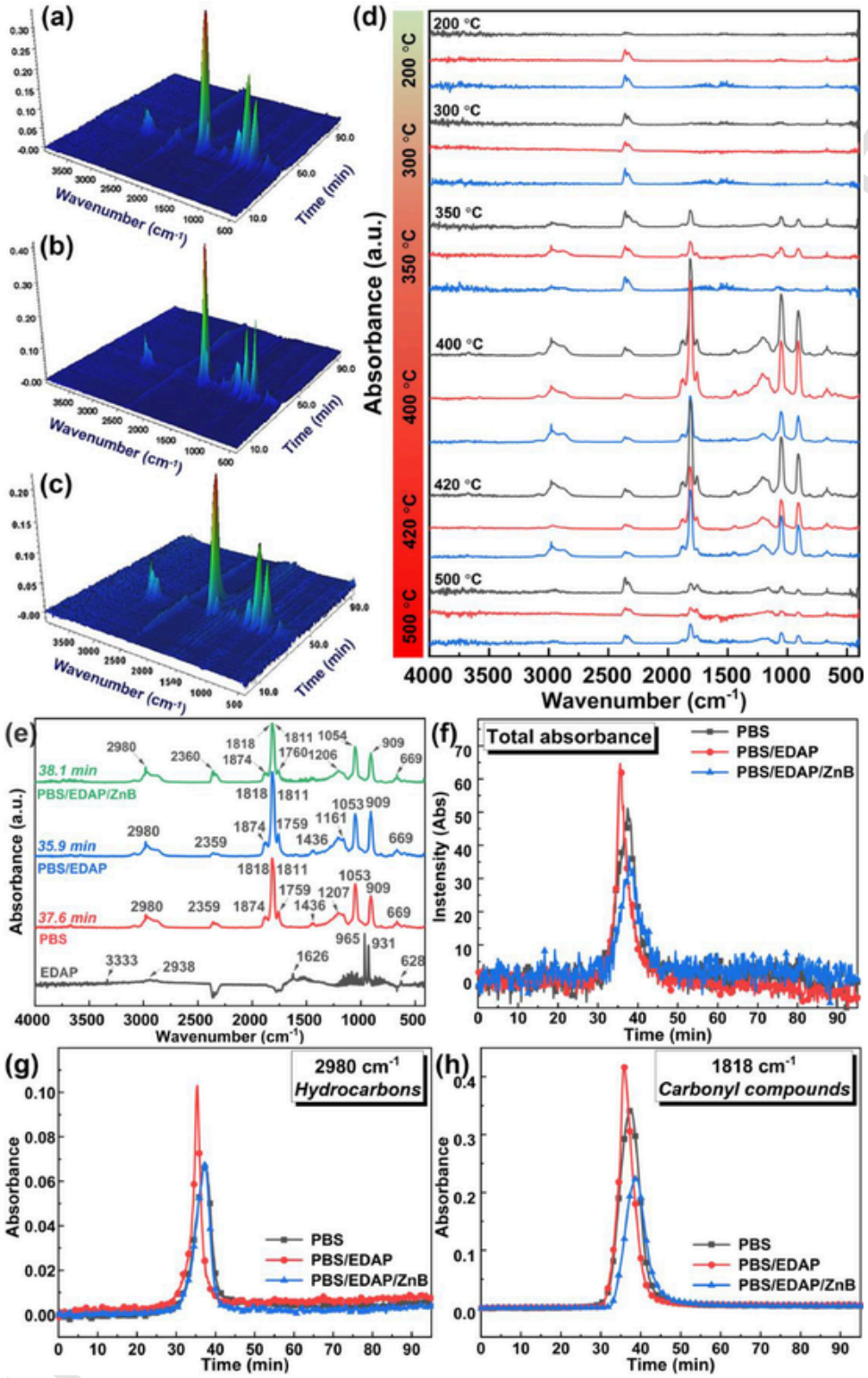

Fig. 10. (a–c) 3D TG-FTIR of PBS, PBS/EDAP, and PBS/EDAP/ZnB; (d) FTIR spectra of gaseous products for neat PBS (blank), PBS/EDAP (red), and PBS/EDAP/ZnB (blue) at different temperatures (200 °C, 300 °C, 350 °C, 400 °C, 420 °C, and 500 °C, respectively); (e) FTIR spectra of EDAP, neat PBS, PBS/EDAP, and PBS/EDAP/ZnB at the maximum evolution rate; (f–h) absorption of pyrolysis products for neat PBS, PBS/EDAP, and PBS/EDAP/ZnB (For interpretation of the references to color in this figure legend, the reader is referred to the web version of this article.).

CRediT authorship contribution statement

Fei Xiao: Writing – original draft, Writing – review & editing. **Gaëlle Fontaine:** Supervision, Writing – original draft, Conceptualization, Writing – review & editing. **Serge Bourbigot:** Supervision, Writing – original draft, Conceptualization, Writing – review & editingFei Xiao: Conceptualization, Methodology, Investigation, Data curation, Software, Formal analysis, Writing – original draft, Writing – review & editing. Gaëlle Fontaine: Supervision, Conceptualization, Methodology,

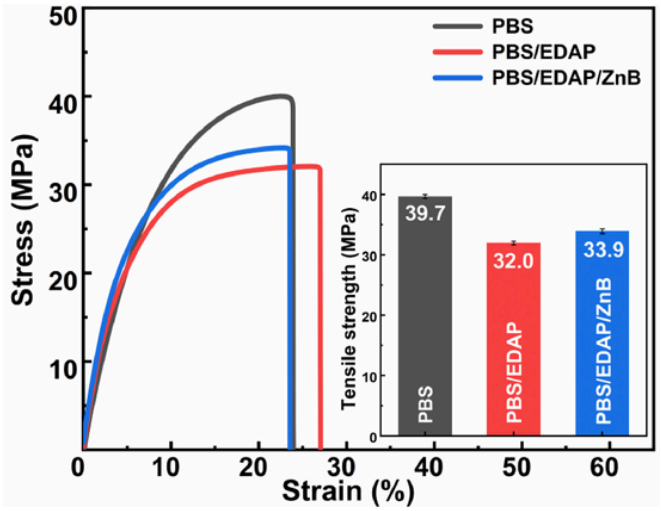

Fig. 11. Stress-strain curves of PBS and its composites from tensile test.

Resources, Project administration, Formal analysis, Writing – review & editing. Serge Bourbigot: Supervision, Conceptualization, Methodology, Resources, Project administration, Formal analysis, Writing – review & editing.

Declaration of Competing Interest

The authors declare that they have no known competing financial interests or personal relationships that could have appeared to influence the work reported in this paper.

Acknowledgments

The authors would like to thank Johan Sarazin, Benjamin Dewailly, and Adeline Marin for the guidance in the measurements, and especially Bertrand Doumert and Bertrand Revel for the support in performing solid-state NMR spectra. Beside, Fei Xiao also gratefully acknowledges the financial support from the China Scholarship Council (*No. 201804910605*).

References

[1] Z. Huang, L. Qian, Q. Yin, N. Yu, T. Liu, D. Tian, Biodegradability studies of poly (butylene succinate) composites filled with sugarcane rind fiber, Polym. Test. 66 (2018) 319–326.
[2] N. Wattanawong, D. Aht-Ong, Antibacterial activity, thermal behavior, mechanical properties and biodegradability of silver zeolite/poly(butylene succinate) composite films, Polym. Degrad. Stab. 183 (2021) 109459.
[3] C. Hu, S. Bourbigot, T. Delaunay, M. Collinet, S. Marcille, G. Fontaine, Poly (isosorbide carbonate): A 'green' char forming agent in polybutylene succinate intumescent formulation, Compos. B. Eng. 184 (2020) 107675.
[4] H. Yang, B. Yu, X. Xu, S. Bourbigot, H. Wang, P. Song, Lignin-derived bio-based flame retardants toward high-performance sustainable polymeric materials, Green Chem. 22 (7) (2020) 2129–2161.
[5] J. Alongi, Z. Han, S. Bourbigot, Intumescence: Tradition versus novelty. A comprehensive review, Prog. Polym. Sci. 51 (2015) 28–73.
[6] S. Bourbigot, M.L. Bras, S. Duquesne, M. Rochery, Recent advances for intumescent polymers, Macromol. Mater. Eng. 289 (6) (2004) 499–511.
[7] G. Fontaine, S. Bourbigot, Intumescent polylactide: a nonflammable material, J. Appl. Polym. Sci. 113 (6) (2009) 3860–3865.
[8] W. He, P. Song, B. Yu, Z. Fang, H. Wang, Flame retardant polymeric nanocomposites through the combination of nanomaterials and conventional flame retardants, Prog. Mater Sci. 114 (2020) 100687.
[9] J. Yue, C. Liu, C. Zhou, X. Fu, L. Luo, L. Gan, X. Yang, J. Huang, Enhancing flame retardancy and promoting initial combustion carbonization via incorporating electrostatically surface-functionalized carbon nanotube synergist into intumescent flame-retardant poly(butylene succinate), Polymer 189 (2020) 122197.
[10] X. Yue, J. Li, P. Liu, W. Pu, Y. Lin, Investigation of flame-retarded poly(butylene succinate) composites using MHSH as synergistic and reinforced agent, J. Mater. Sci. 53 (7) (2017) 5004–5015.
[11] Y. Wang, C. Liu, X. Shi, J. Liang, Z. Jia, G. Shi, Synergistic effect of halloysite nanotubes on flame resistance of intumescent flame retardant poly(butylene succinate) composites, Polym. Compos. 40 (1) (2019) 202–209.
[12] L. Liu, G. Huang, P. Song, Y. Yu, S. Fu, Converting industrial alkali lignin to biobased functional additives for improving fire behavior and smoke suppression of polybutylene succinate, ACS Sustain. Chem. Eng. 4 (9) (2016) 4732–4742.
[13] G. Camino, L. Costa, M.P. Luda di Cortemiglia, Overview of fire retardant mechanisms, Polym. Degrad. Stab. 33 (2) (1991) 131–154.
[14] Y. Wang, C. Liu, J. Lai, C. Lu, X. Wu, Y. Cai, L. Gu, L. Yang, G. Zhang, G. Shi, Soy protein and halloysite nanotubes-assisted preparation of environmentally friendly intumescent flame retardant for poly (butylene succinate), Polym. Test. 81 (2020) 106174.
[15] Y. Sun, S. Sun, L. Chen, L. Liu, P. Song, W. Li, Y. Yu, L. Fengzhu, J. Qian, H. Wang, Flame retardant and mechanically tough poly (lactic acid) biocomposites via combining ammonia polyphosphate and polyethylene glycol, Compos. Commun. 6 (2017) 1–5.
[16] Y. Zhang, J. Jing, T. Liu, L. Xi, T. Sai, S. Ran, Z. Fang, S. Huo, P. Song, A molecularly engineered bioderived polyphosphate for enhanced flame retardant, UV-blocking and mechanical properties of poly (lactic acid), Chem. Eng. J. 411 (2021) 128493.
[17] F. Xiao, G. Fontaine, S. Bourbigot, Recent developments in fire retardancy of polybutylene succinate, Polym. Degrad. Stab. 183 (2021) 109466.
[18] X. Wang, L. Song, H. Yang, H. Lu, Y. Hu, Synergistic effect of graphene on antidripping and fire resistance of intumescent flame retardant poly(butylene succinate) composites, Ind. Eng. Chem. Res. 50 (9) (2011) 5376–5383.
[19] C. Hu, S. Bourbigot, T. Delaunay, M. Collinet, S. Marcille, G. Fontaine, Synthesis of isosorbide based flame retardants: application for polybutylene succinate, Polym. Degrad. Stab. 164 (2019) 9–17.
[20] H. Yang, L. Song, Q. Tai, X. Wang, B. Yu, Y. Yuan, Y. Hu, R.K.K. Yuen, Comparative study on the flame retarded efficiency of melamine phosphate, melamine phosphite and melamine hypophosphite on poly(butylene succinate) composites, Polym. Degrad. Stab. 105 (2014) 248–256.
[21] Z. Shao, C. Deng, Y. Tan, M. Chen, L. Chen, Y. Wang, Flame retardation of polypropylene via a novel intumescent flame retardant: ethylenediamine-modified ammonium polyphosphate, Polym. Degrad. Stab. 106 (2014) 88–96.
[22] J. Davis, M. Huggard, The technology of halogen-free flame retardant phosphorus additives for polymeric systems, J. Vinyl Addit. Technol. 2 (1) (1996) 69–75.
[23] H.J. Kruger, W.W. Focke, W. Mhike, A. Taute, A. Roberson, Thermal properties of polyethylene flame retarded with expandable graphite and intumescent fire retardant additives, Fire Mater. 41 (6) (2017) 573–586.
[24] B. Lecouvet, M. Sclavons, C. Bailly, S. Bourbigot, A comprehensive study of the synergistic flame retardant mechanisms of halloysite in intumescent polypropylene, Polym. Degrad. Stab. 98 (11) (2013) 2268–2281.
[25] Z. Ma, X. Liu, X. Xu, L. Liu, B. Yu, C. Maluk, G. Huang, H. Wang, P. Song, Bioinspired, highly adhesive, nanostructured polymeric coatings for superhydrophobic fire-extinguishing thermal insulation foam, ACS Nano 15 (7) (2021) 11667–11680.
[26] T. Sai, S. Ran, Z. Guo, H. Yan, Y. Zhang, H. Wang, P. Song, Z. Fang, Transparent, highly thermostable and flame retardant polycarbonate enabled by rod-like phosphorous-containing metal complex aggregates, Chem. Eng. J. 409 (2021) 128223.
[27] Y. Chen, J. Zhan, P. Zhang, S. Nie, H. Lu, L. Song, Y. Hu, Preparation of intumescent flame retardant poly (butylene succinate) using fumed silica as synergistic agent, Ind. Eng. Chem. Res. 49 (17) (2010) 8200–8208.
[28] S. Zhang, Y. Li, J. Guo, L. Gu, H. Li, B. Fei, J. Sun, X. Gu, Preparation of hexakis (4-aldehyde phenoxy) cyclotriphosphazene grafted kaolinite and its synergistic fire resistance in poly (butylene succinate), Polym. Compos. (2019).
[29] Y. Wang, S. Zhang, X. Wu, C. Lu, Y. Cai, L. Ma, G. Shi, L. Yang, Effect of montmorillonite on the flame-resistant and mechanical properties of intumescent flame-retardant poly(butylene succinate) composites, J. Therm. Anal. Calorim. 128 (3) (2017) 1417–1427.
[30] Y. Wang, C. Liu, J. Lai, C. Lu, X. Wu, Y. Cai, L. Gu, L. Yang, G. Zhang, G. Shi, Soy protein and halloysite nanotubes-assisted preparation of environmentally friendly intumescent flame retardant for poly(butylene succinate), Polym. Test. 81 (2020) 106174.
[31] Y. Zhang, Y. Hu, J. Wang, W. Tian, K.M. Liew, Y. Zhang, B. Wang, Engineering carbon nanotubes wrapped ammonium polyphosphate for enhancing mechanical and flame retardant properties of poly (butylene succinate), Compos. Part A Appl. Sci. Manuf. 115 (2018) 215–227.
[32] M. Jiang, Y. Zhang, Y. Yu, Q. Zhang, B. Huang, Z. Chen, T. Chen, J. Jiang, Flame retardancy of unsaturated polyester composites with modified ammonium polyphosphate, montmorillonite, and zinc borate, J. Appl. Polym. Sci. 136 (11) (2019) 47180.
[33] F. Carpentier, S. Bourbigot, M.L. Bras, R. Delobel, M. Foulon, Charring of fire retarded ethylene vinyl acetate copolymer -magnesium hydroxide/zinc borate formulations, Polym. Degrad. Stab. 69 (1) (2000) 83–92.
[34] L.A. Savas, M. Dogan, Flame retardant effect of zinc borate in polyamide 6 containing aluminum hypophosphite, Polym. Degrad. Stab. 165 (2019) 101–109.
[35] M.A. Oualha, N. Amdouni, F. Laoutid, Synergistic flame-retardant effect between calcium hydroxide and zinc borate in ethylene-vinyl acetate copolymer (EVA), Polym. Degrad. Stab. 144 (2017) 315–324.
[36] S. Yang, G. Lv, Y. Liu, Q. Wang, Synergism of polysiloxane and zinc borate flame retardant polycarbonate, Polym. Degrad. Stab. 98 (12) (2013) 2795–2800.
[37] C. Hoffendahl, G. Fontaine, S. Duquesne, F. Taschner, M. Mezger, S. Bourbigot, The combination of aluminum trihydroxide (ATH) and melamine borate (MB) as fire retardant additives for elastomeric ethylene vinyl acetate (EVA), Polym. Degrad. Stab. 115 (2015) 77–88.
[38] S. Bourbigot, J. Sarazin, T. Bensabath, Intumescent polypropylene in extreme fire conditions, Fire Saf. J. (2020) 103082.

[39] S. Bourbigot, G. Fontaine, A. Gallos, S. Bellayer, Reactive extrusion of PLA and of PLA/carbon nanotubes nanocomposite: processing, characterization and flame retardancy, Polym. Adv. Technol. 22 (1) (2011) 30–37.
[40] S. Bourbigot, J. Sarazin, F. Samyn, M. Jimenez, Intumescent ethylene-vinyl acetate copolymer: reaction to fire and mechanistic aspects, Polym. Degrad. Stab. 161 (2019) 235–244.
[41] H. Vahabi, B.K. Kandola, M.R. Saeb, Flame retardancy index for thermoplastic composites, Polymers 11 (3) (2019) 407.
[42] C. Hoffendahl, G. Fontaine, S. Duquesne, F. Taschner, M. Mezger, S. Bourbigot, The fire retardant mechanism of ethylene vinyl acetate elastomer (EVM) containing aluminium trihydroxide and melamine phosphate, RSC Adv. 4 (39) (2014) 20185–20199.
[43] L. Geoffroy, F. Samyn, M. Jimenez, S. Bourbigot, Innovative 3D printed design to conceive highly fire-retardant multi-material, Polym. Degrad. Stab. 169 (2019) 108992.
[44] A. Ramgobin, G. Fontaine, S. Bourbigot, A case study of polyether ether ketone (I): investigating the thermal and fire behavior of a high-performance material, Polymers 12 (8) (2020) 1789.
[45] B. Schartel, T.R. Hull, Development of fire-retarded materials-Interpretation of cone calorimeter data, Fire Mater. 31 (5) (2007) 327–354.
[46] J. Yue, C. Liu, C. Zhou, X. Fu, L. Luo, L. Gan, X. Yang, J. Huang, Enhancing flame retardancy and promoting initial combustion carbonization via incorporating electrostatically surface-functionalized carbon nanotube synergist into intumescent flame-retardant poly (butylene succinate), Polymer 189 (2020) 122197.
[47] D.-Y. Wang, Y. Liu, Y.-Z. Wang, C.P. Artiles, T.R. Hull, D. Price, Fire retardancy of a reactively extruded intumescent flame retardant polyethylene system enhanced by metal chelates, Polym. Degrad. Stab. 92 (8) (2007) 1592–1598.
[48] B. Sundström, The Development of a European Fire Classification System for Building Products-test Methods and Mathematical Modelling, Lund University, 2007.
[49] A.B. Morgan, W. Liu, Flammability of thermoplastic carbon nanofiber nanocomposites, Fire Mater. 35 (1) (2011) 43–60.
[50] B. Du, Z. Fang, Effects of carbon nanotubes on the thermal stability and flame retardancy of intumescent flame-retarded polypropylene, Polym. Degrad. Stab. 96 (10) (2011) 1725–1731.
[51] T. Kashiwagi, F. Du, J.F. Douglas, K.I. Winey, R.H. Harris, J.R. Shields, Nanoparticle networks reduce the flammability of polymer nanocomposites, Nat. Mater. 4 (12) (2005) 928–933.
[52] W.-H. Rao, W. Liao, H. Wang, H.-B. Zhao, Y.-Z. Wang, Flame-retardant and smoke-suppressant flexible polyurethane foams based on reactive phosphorus-containing polyol and expandable graphite, J. Hazard. Mater. 360 (2018) 651–660.
[53] J. Sarazin, C.A. Davy, S. Bourbigot, G. Tricot, J. Hosdez, D. Lambertin, G. Fontaine, Flame resistance of geopolymer foam coatings for the fire protection of steel, Compos. B Eng. 222 (2021) 109045.
[54] C. Hoffendahl, S. Duquesne, G. Fontaine, F. Taschner, M. Mezger, S. Bourbigot, Decomposition mechanism of fire retarded ethylene vinyl acetate elastomer (EVA) containing aluminum trihydroxide and melamine, Polym. Degrad. Stab. 113 (2015) 168–179.
[55] N. Hansupo, G. Tricot, S. Bellayer, P. Roussel, F. Samyn, S. Duquesne, M. Jimenez, M. Hollman, P. Catala, S. Bourbigot, Getting a better insight into the chemistry of decomposition of complex flame retarded formulation: new insights using solid state NMR, Polym. Degrad. Stab. 153 (2018) 145–154.
[56] C. Mercier, L. Montagne, H. Sfihi, G. Palavit, J.C. Boivin, A.P. Legrand, Local structure of zinc ultraphosphate glasses containing large amount of hydroxyl groups: 31P and 1H solid state nuclear magnetic resonance investigation, J. Non Cryst. Solids 224 (2) (1998) 163–172.
[57] F. Samyn, S. Bourbigot, S. Duquesne, R. Delobel, Effect of zinc borate on the thermal degradation of ammonium polyphosphate, Thermochim. Acta 456 (2) (2007) 134–144.
[58] A. Sut, S. Greiser, C. Jäger, B. Schartel, Interactions in multicomponent flame-retardant polymers: solid-state NMR identifying the chemistry behind it, Polym. Degrad. Stab. 121 (2015) 116–125.
[59] S. Bourbigot, M.L. Bras, R. Delobel, R. Decressain, J.-P. Amoureux, Synergistic effect of zeolite in an intumescence process: study of the carbonaceous structures using solid-state NMR, J. Chem. Soc. Faraday Trans. 92 (1) (1996) 149–158.
[60] A. Karrasch, E. Wawrzyn, B. Schartel, C. Jäger, Solid-state NMR on thermal and fire residues of bisphenol A polycarbonate/silicone acrylate rubber/bisphenol A bis (diphenyl-phosphate)/(PC/SiR/BDP) and PC/SiR/BDP/zinc borate (PC/SiR/BDP/ZnB)–part I: PC charring and the impact of BDP and ZnB, Polym. Degrad. Stab. 95 (12) (2010) 2525–2533.
[61] Q.F. Gillani, F. Ahmad, M.A. Mutalib, P.S. Megat-Yusoff, S. Ullah, P.J. Messet, M. Zia-ul-Mustafa, Thermal degradation and pyrolysis analysis of zinc borate reinforced intumescent fire retardant coatings, Prog. Org. Coat. 123 (2018) 82–98.
[62] U. Braun, B. Schartel, M.A. Fichera, C. Jäger, Flame retardancy mechanisms of aluminium phosphinate in combination with melamine polyphosphate and zinc borate in glass-fibre reinforced polyamide 6,6, Polym. Degrad. Stab. 92 (8) (2007) 1528–1545.
[63] F. Ngohang, G. Fontaine, L. Gay, S. Bourbigot, Revisited investigation of fire behavior of ethylene vinyl acetate/aluminum trihydroxide using a combination of mass loss cone, Fourier transform infrared spectroscopy and electrical low pressure impactor, Polym. Degrad. Stab. 106 (2014) 26–35.
[64] X. Zhao, D. Xiao, J.P. Alonso, D.-Y. Wang, Inclusion complex between beta-cyclodextrin and phenylphosphonicdiamide as novel bio-based flame retardant to epoxy: Inclusion behavior, characterization and flammability, Mater. Des. 114 (2017) 623–632.
[65] H. Luo, W. Rao, P. Zhao, L. Wang, Y. Liu, C. Yu, An efficient organic/inorganic phosphorus–nitrogen–silicon flame retardant towards low-flammability epoxy resin, Polym. Degrad. Stab. 178 (2020) 109195.
[66] W.-Y. Chen, Y.-Z. Wang, F.-C. Chang, Thermal and flame retardation properties of melamine phosphate-modified epoxy resins, Journal of Polymer Research 11 (2) (2004) 109–117.
[67] Q.F. Gillani, F. Ahmad, M.I. Abdul Mutalib, P.S.M. Megat-Yusoff, S. Ullah, P.J. Messet, M. Zia-ul-Mustafa, Thermal degradation and pyrolysis analysis of zinc borate reinforced intumescent fire retardant coatings, Prog. Org. Coat. 123 (2018) 82–98.
[68] Y. Jin, G. Huang, D. Han, P. Song, W. Tang, J. Bao, R. Li, Y. Liu, Functionalizing graphene decorated with phosphorus-nitrogen containing dendrimer for high-performance polymer nanocomposites, Compos. Part A Appl. Sci. Manuf. 86 (2016) 9–18.
[69] Y.F. Shih, Thermal degradation and kinetic analysis of biodegradable PBS/multiwalled carbon nanotube nanocomposites, J. Polym. Sci. Part B Polym. Phys. 47 (13) (2009) 1231–1239.
[70] X. Wang, Y. Hu, L. Song, H. Yang, B. Yu, B. Kandola, D. Deli, Comparative study on the synergistic effect of POSS and graphene with melamine phosphate on the flame retardance of poly(butylene succinate), Thermochim. Acta 543 (2012) 156–164.
[71] G. Huang, W. Chen, T. Wu, H. Guo, C. Fu, Y. Xue, K. Wang, P. Song, Multifunctional graphene-based nano-additives toward high-performance polymer nanocomposites with enhanced mechanical, thermal, flame retardancy and smoke suppressive properties, Chem. Eng. J. 410 (2021) 127590.
[72] X. Lai, S. Tang, H. Li, X. Zeng, Flame-retardant mechanism of a novel polymeric intumescent flame retardant containing caged bicyclic phosphate for polypropylene, Polym. Degrad. Stab. 113 (2015) 22–31.
[73] B. Tawiah, B. Yu, R.K. Yuen, Y. Hu, R. Wei, J.H. Xin, B. Fei, Highly efficient flame retardant and smoke suppression mechanism of boron modified graphene Oxide/Poly (Lactic acid) nanocomposites, Carbon 150 (2019) 8–20.
[74] L. Liu, M. Zhu, Y. Shi, X. Xu, Z. Ma, B. Yu, S. Fu, G. Huang, H. Wang, P. Song, Functionalizing MXene towards highly stretchable, ultratough, fatigue-and fire-resistant polymer nanocomposites, Chem. Eng. J. (2021) 130338.
[75] Q. Liu, Y. Wu, F. Xing, Q. Liu, X. Guo, C. Huang, B2O3@ BPO4 sandwich-like hollow spheres as metal-free supported liquid-phase catalysts, J. Catal. 381 (2020) 599–607.
[76] M. Dogan, S.M. Unlu, Flame retardant effect of boron compounds on red phosphorus containing epoxy resins, Polym. Degrad. Stab. 99 (2014) 12–17.
[77] T. Nageswara Rao, T.M. Naidu, M.S. Kim, B. Parvatamma, Y. Prashanthi, B. Heun Koo, Influence of zinc oxide nanoparticles and char forming agent polymer on flame retardancy of intumescent flame retardant coatings, Nanomaterials 10 (1) (2020) 42.
[78] Y. Wang, C. Liu, X. Shi, J. Liang, Z. Jia, G. Shi, Synergistic effect of halloysite nanotubes on flame resistance of intumescent flame retardant poly (butylene succinate) composites, Polym. Compos. 40 (1) (2019) 202–209.
[79] R. Jeencham, N. Suppakarn, K. Jarukumjorn, Effect of flame retardants on flame retardant, mechanical, and thermal properties of sisal fiber/polypropylene composites, Compos. B Eng. 56 (2014) 249–253.